Journal of Radiation and Nuclear Applications
An International Journal

http://dx.doi.org/10.18576/jrna/090312

Utilizing the Gamma-Ray Spectrometric and Magnetic Methods for Determining the Radioactive Anomalies and Their Relation to the Subsurface Structures, Wadi Hammad and vicinity area, North Eastern Desert, Egypt

Mohamed A. Shaheen[*]

Nuclear Materials Authority, P.O. Box 530 El-Maadi, Cairo, Egypt.

Received: 2 Jun. 2024, Revised: 22 Jul. 2024, Accepted: 1 Aug. 2024.

Published online: 1 Sep 2024

Abstract: Metamorphic, igneous, and sedimentary rocks of many sorts are present in the area under consideration. The primary objectives of this study are to identify the structural pattern and define the highly radioactive zones in the Wadi Hammad and vicinity area using data from an airborne survey. The examined area's total count, eU, and eTh maps show a wide range of radioactivity, with values ranging roughly from 2 to 20 Ur, 0.1 to 13 ppm, and 1 to 32 ppm respectively. The highly white color seen in the radioelement composite image, which denotes a rise in the concentrations of the three radioelements in the northwest, center, and east of the area under investigation, is primarily associated with older granite, younger granite, and post-granitic dykes. Through integration between the residual and geology of the researched area, surface lineament evaluations were performed. This integration offered solid proof that two sets of faults have NE-SW and NW-SE trending directions. To eliminate the local magnetic impact, the total aeromagnetic intensity data was decreased to the north magnetic pole (RTP). The power spectrum approach was applied to the RTP data to determine the various magnetic wavelengths of the regional and residual magnetic components. Advanced approaches were also used to reference the RTP data for structural interpretation and depth estimation. These techniques include upward continuation, Werner, and the Gm-Sys modeling tool. For the regional and residual components, the power spectrum curve displays two linear segments at 1800 and 800 m, respectively. While the residual map has trended ENE, WNW, NE, and NS, the interpretation of RTP for the regional aeromagnetic map has almost trended ENE and NW. According to the magnetic modeling, the basement's greatest depth is close to 1500 m, and it gets deeper as you move away from the basin's southwest. The research area is influenced by prominent structural components such as faults and lithological contacts. These components mostly target NNW and NNE trends. There is an agreement between the structural lineaments and high radioactive zones.

Keywords: Wadi Hammad; Spectral Gamma-ray; North Eastern Desert; Radioactive Anomaly.

1 Introduction

The study area (Fig. 1) represents the African Orogenic belt, which was separated from the Arabian Shield by the Red Sea graben. It is a part of the North Eastern Desert of Egypt that was subjected to several activities in the Precambrian rocks due to its long history and highly varied complicated geology. It comprises a variety of sedimentary, metamorphic, and igneous rocks.

It is bounded by latitudes 27^{o} 02′ to 27^{o} 22′ N and longitudes 32^{o} 40′ to 32^{o} 60′ E (Fig. 2).

Mapping geological structures depends mainly on the results of magnetic surveys, and this is considered one of the most important geological applications of magnetic surveys **[**1**]**.

Magnetic methods help in prospecting for different minerals by identifying different geological structures such as fractures, faults, and folds, which can be determined by interpreting the different magnetic anomalies. The main objective of this study is to determine the geological structures in the study area that may be closely related to the distribution of radioactive elements in the area.

[*]Corresponding author e-mail: mamshaheen2002@yahoo.com

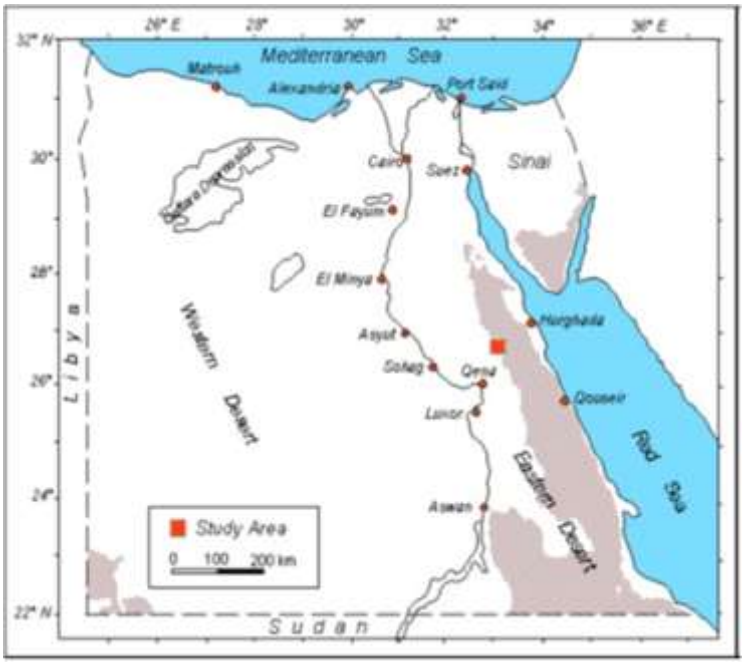

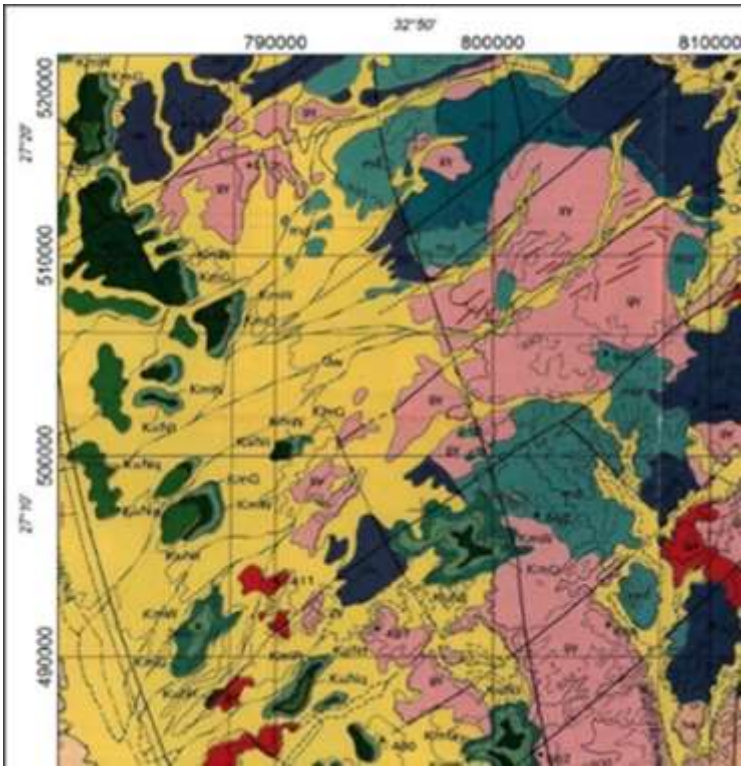

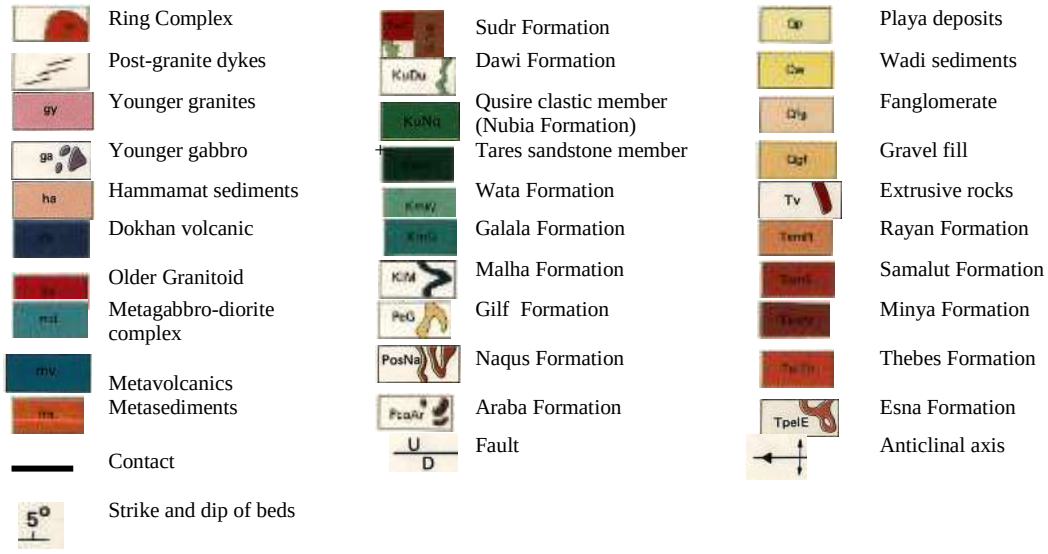

Fig.2: Geological, map of Wadi Hammad and vicinity area North, Eastern Desert, Egypt after [2].

2 Geological Setting

2.1 The basement complex

The Wadi Hammed and Wadi Qena areas are located in the Central Eastern Desert (CED) of Egypt. The basement rocks exposed in the study area have been investigated by many authors **[**3, 4]. They are represented by metasediments, metavolcanic, meta gabbro-diorites complex, older granitoid, Dokhan Volcanics, Hammamat sediments, younger gabbro and younger granites dissected by post-granite dykes, and a tertiary ring complex.

The basement rocks are non-conformably overlain by a sedimentary cover of Cretaceous Nubian Formation to Miocene sediments, started by the Araba Formation to Rayan Formation (Fig. 2). The metasediments are fine-to very fine-grained, highly altered, foliated, lineated and composed mainly of schist, greywacke, and mudstone.

Metavolcanics are composed of a thick sequence of stratified lava flows ranging in composition from basic to acidic verities interbedded with pyroclastics. These rocks crop out in the northern and central parts of the study area.

The meta gabbro-diorite complex is found in isolated outcrops in the northern and eastern parts of the study area. They have low to moderate relief, are coarse-grained, and range in color from dark grey to black. The older granitoids are tonalite-granodiorite in composition.

They occur as small, scattered masses in the eastern and western parts of the mapped area. They have low to moderate relief, are coarse-grained, and vary from

light grey to whitish-gray. Dokhan Volcanics are primarily composed of basic to acidic lava flows interbedded with pyroclastics of tuffs, lapilli tuffs, and agglomerates.

They are interbedded with Hammamat sediments **[**5, 6**]**. They vary in color from black to gray, buff, reddish brown, and red, with various shades of purple and brown.

The basement rocks were exposed to intensive erosion, and sediments of molasse (Hammamat) character were deposited in the basins**[**7, 8**]**. The Hammamat sediments occupy the eastern part of the study area and are composed mainly of conglomerate, sandstone, greywackes, and siltstones. Younger gabbro occurs as medium-grained, compact, hard, black to greenish-black in color and shows a boulder appearance. The younger granite ranges in composition from monzogranite to syenogranite in the area under investigation. It is the most dominant rock as mentioned in the study area (Fig. 2). They have moderate to high relief and vary in color from red to reddish brown and pinkish. The post-granite dykes took place along fractures and/or fissures, especially in both the NE and ENE directions. They are dominated by dolerite, andesite, and felsite dykes **[**7**]**. Ring complexes are successive ring-like intrusions. They are of gabbroic rock, nepheline syenite, and alkaline granite **[**9**]**.

2.2 Mesozoic cover sediments

(a) Nubian Formation:

Intercalated sediments such as shale, marl, sandstone, limestone, and phosphate bands dominate the Upper Cretaceous sedimentary cover. These sediments are composed of grey, yellowish-grey, and brown-gray quartz sandstones **[**10, 11**]**.

(b) Quaternary sediments:

In the area under investigation, the Upper Neogene and Lower Quaternary rocks form large detrital cones that are spatially confined to the near-mouth areas of the main

Wadies. They are made up of boulders, pebbles, and sandy detrital material. Middle Quaternary and Holocene Wadi deposits are widely spread in the plain part of Wadi Qena and the large wadies. They are represented by detrital pebble, sandy-clayey, and boulder formations [10, 11].

3 Airborne Survey

3.1. Gamma-Ray Survey

The most common applications for spectral gamma-ray surveys are radioactive mineral exploration and geological and geochemical mapping. A gamma-ray survey was also carried out for environmental studies to assess the risk of radon [12, 13, 14, 15 & 16].

3.2. Airborne Magnetic Survey

There are many geological applications of magnetic surveys. The most important one is mapping the geological structures in the study area such as faults, fractures, and folds to which mineral deposits are related.

3.3. Data Collection

In 1984, the American Western Geophysical Company, represented by the Air Services Division, carried out radioactive and magnetic aerial geophysical surveys in parallel lines in the direction northeast-southwest, so that they were perpendicular to the directions of the common geological structures in the study area. The measurements were made with equal distances between the scan lines of 1 km, while the distances between the connecting lines were 10 km in the direction of Northwest-Southeast.

A high-sensitivity, 256-channel Picodas gamma-ray spectrometer was placed in the aircraft to conduct the gamma-ray scan. Three crystal boxes (A, B, and C) with a combined volume of 3000 cubic inches make up the detecting package (50 L). There are two detectors in this detection kit. The first detector, the high-sensitivity NaI, has 12 detectors to measure the various energies of terrestrial radiation for the three main elements (K, U, and Th), while the second detector, the high-sensitivity NaI, has one detector to measure the specific energy of cosmic and atmospheric radiation. To properly adjust the strength of the detectors, a software program was used to track the photo-peak of gamma emitters, typically potassium and thorium (auto-tuning). Additionally, a Varian "V-85" high-sensitivity (0.1 nT) airborne magnetometer and a proton free-precession sensor were used to conduct the magnetic survey [17].

4 Discussion and Interpretation

4.1. Airborne Gamma-Ray Data Interpretation

a) Maps of total count and radioelements

The strong agreement between the overall pattern of the recorded measurements and the surface distribution of the various types of rock units is a key component in the qualitative interpretation of ground gamma-ray survey data. The texture of the gamma-ray contour lines and their signatures in the total-count, K, eU, and eTh produced maps may help interpret the surface geology (lithology and structure) of the studied area.

In the study area, the total count and the three radioelements (K, eU, and eTh) concentration measurements were represented by color image maps (Figs. 3, 4, 5, and 6). These maps could show-at a glance-that the distribution of the high radioactivity level is highly controlled by older granitoid, younger granites, and post-granitic dykes that are exposed on the surface in the northern part, southeastern part, and eastern part of the study area. The major trend from the four radiometric maps is the NNW-SSE trend.

In general, the surveyed area's total count, eU, and eTh maps show a wide range of radioactivity, ranging from about 2 to 20 Ur, 1 to 13 ppm, and 1 to 32 ppm, respectively. These wide ranges, when compared to the geologic map of the area (Fig. 2), reflect different radioactivity levels within and between the different rock types in the area. Generally, the three maps can be divided into three zones with overlapped radioactivity levels. The first is low-level radioactivity, which is recorded over the Dokhan volcanic, metavolcanic, Metasediments, Qusire Clastic member (Nubia Formation), and Tares sandstone member.

The second is the intermediate radioactivity zone, which is represented by the Metagabbro-Diorite complex, Hammamat sediments, and Dawi formation. The third and highest radioactivity zone is associated with younger granitoid granites and post-granitic dykes. On the other hand, the potassium map shows a medium range of concentrations (from 0.2 to 4 %) all over the exposed rock units in the study area. Despite this range, there is good agreement with the previous total count, eU, and eTh maps concerning the highest and lowest levels and the distribution of the radiation anomalies.

b. Maps of radioelement ratios

The surface shape, percentage of the outcrop, inversion trapping of radon, and other absorbers such as soil moisture and vegetation have less of an impact on the radioelement ratio maps of eU/eTh and eU/K. As a result, the ratio maps are more typically indicative of lithological units or geological-geochemical environments than the absolute intensity and concentration maps alone, making them particularly helpful in the interpretation of the ground gamma-ray spectrometry findings. These maps serve as a diagnostic tool for locating unusual U concentration zones from an exploratory perspective [18, 19].

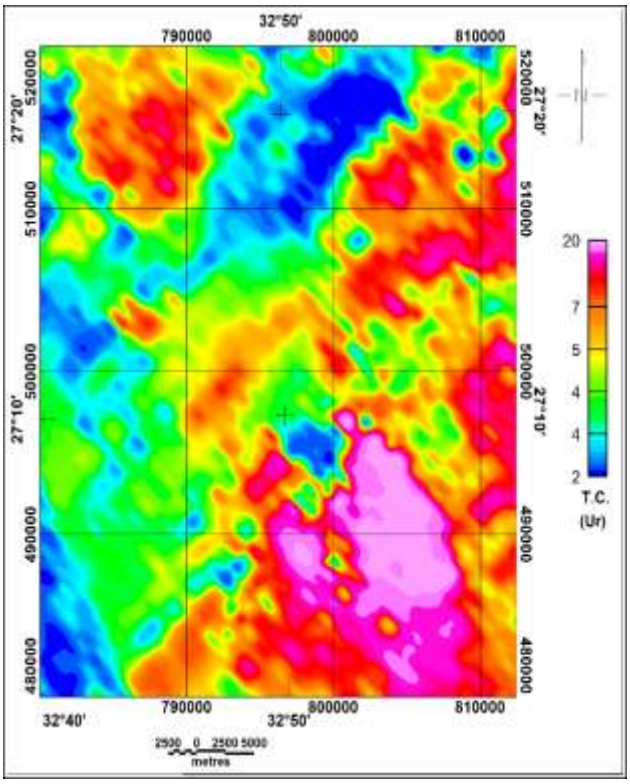

Fig.3: Total-count filled colored contour map (in Ur), Wadi Hammad and vicinity area North Eastern Desert, Egypt.

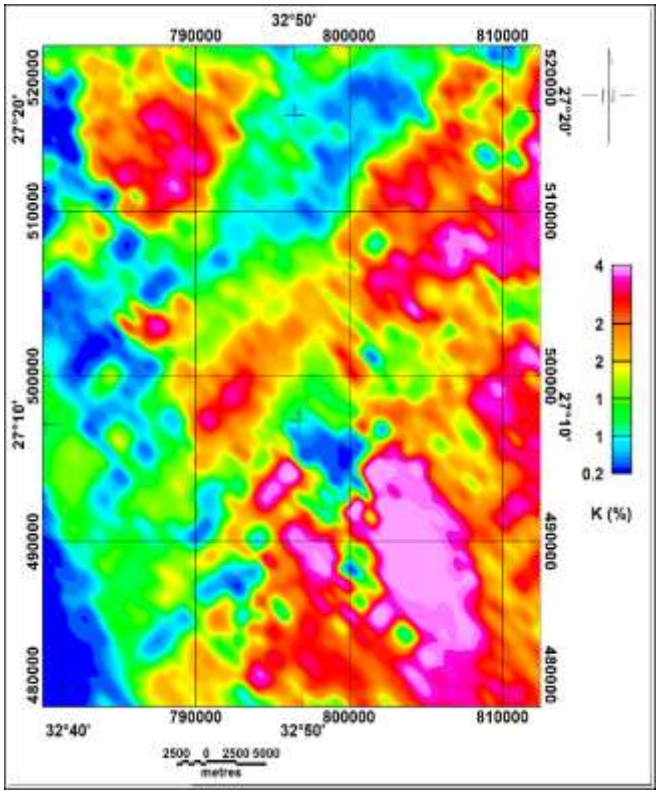

Fig.4: Potassium-filled colored contour map in (%), Wa Hammad and vicinity area North Eastern Desert, Egypt.

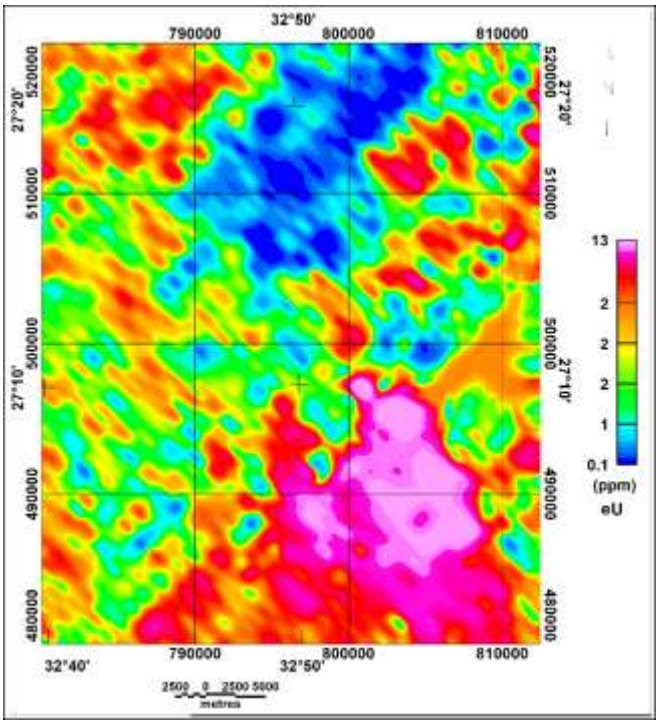

Fig. 5: Equivalent uranium-filled colored contour map (in ppm), Wadi Hammad and vicinity area North Eastern Desert, Egypt.

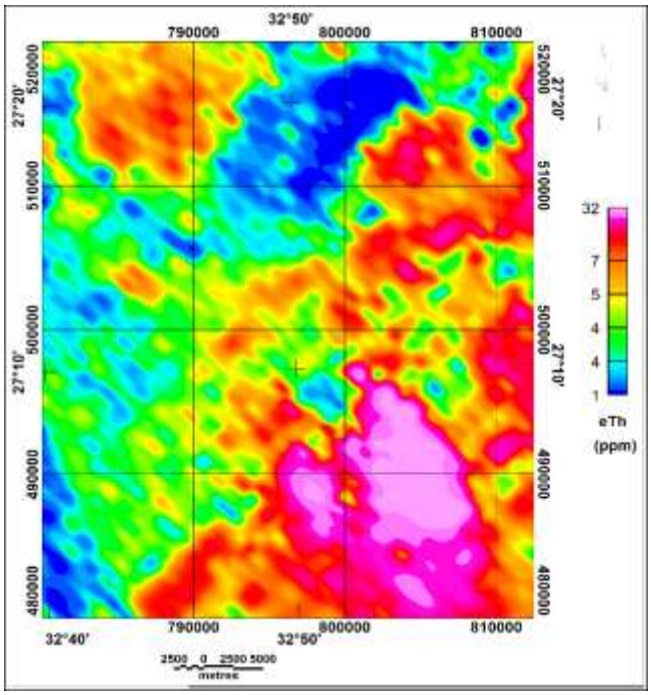

Fig. 6: Equivalent thorium-filled colored contour map (in ppm), Wadi Hammad and vicinity area North Eastern Desert, Egypt.

The western and central regions of the research area had greater eU/eTh values than their surroundings, which suggests U enrichment, according to the eU/eTh ratio map of the area (Fig. 7). These abnormal components might have developed as a result of the existence of solutions that were heavily enriched in U, which mobilize more quickly than Th. In contrast, the eU/K ratio map (Fig. 8) validates the majority of the abnormal eU/eTh portions and displays extremely high values (which can reach 3) in several areas of the investigated area.

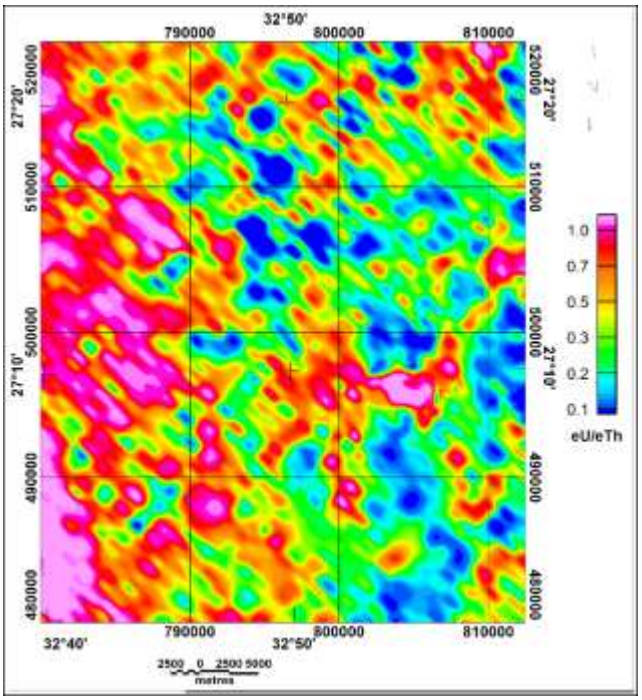

Fig.7: eU/eTh filled colored contour map (in ppm/ppm), Wadi Hammad and vicinity area North Eastern Desert, Egypt.

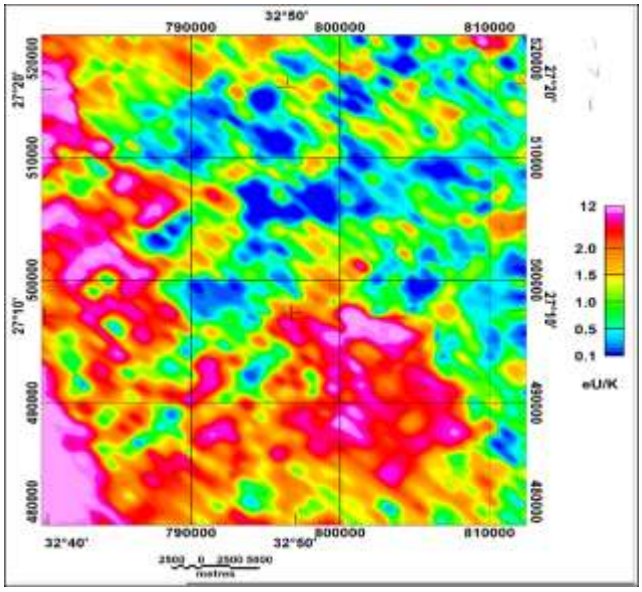

Fig. 8: eU/K filled colored contour map (in ppm/ %), Wadi Hammad and vicinity area North Eastern Desert, Egypt.

c) Maps of ternary radioelements

1) Radioelement composite image in false color

It is identified as an absolute radioelement K, eU, and eTh composite picture. This composite image was created using the color combination of red, blue, and green (RBG) (Fig. 9). This shows that the Dokhan volcanic, metavolcanic, Metasediments, Qusire Clastic member (Nubia Formation), and Tares sandstone member are all closely associated to the dark color, which implies low concentrations of three radioelements throughout the mapped area. Green and violet hues, which indicate intermediate amounts of the three radioactive elements, are linked to the Metagabbro-Diorite Complex, Hammamat deposits,

and Dawi formation. The northern, central, and eastern portions of the area under research are highly white, which denotes a rise in the concentrations of the three radioelements, and is mainly related to older granitoid, younger granites, and post-granitic dykes.

2) Composite image of uranium in false colors

According to the chosen parameters, eU concentration zones are shown as parts of white light. As seen in the illustration in Fig (10). In the northern, central, and eastern parts of the research region, the white light portions are primarily connected to older granitoid, younger granites,

and post-granitic dykes. All around the landscape, there are also sporadic smaller white sections. According to **[**19**]**,

these areas can be seen as reflecting good geochemical settings that are suitable for the creation of U deposits, and they can therefore be utilized as exploration guides to look for more surface and subsurface U-mineralization.

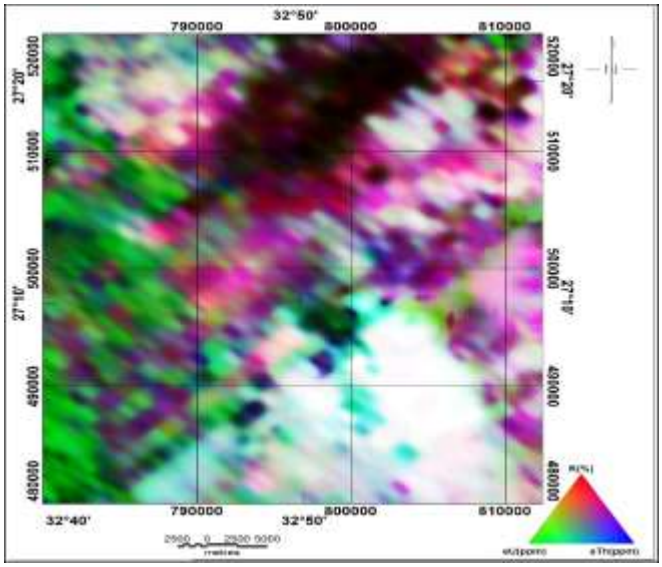

Fig.9: Radioelement composite image, Wadi Hammad and vicinity area North Eastern Desert, Egypt.

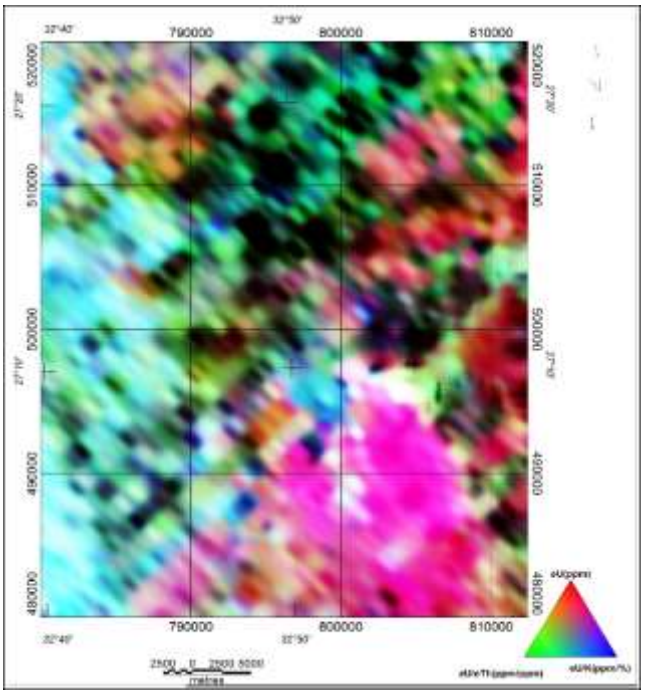

Fig.10: Uranium composite image, Wadi Hammad and vicinity area North Eastern Desert, Egypt.

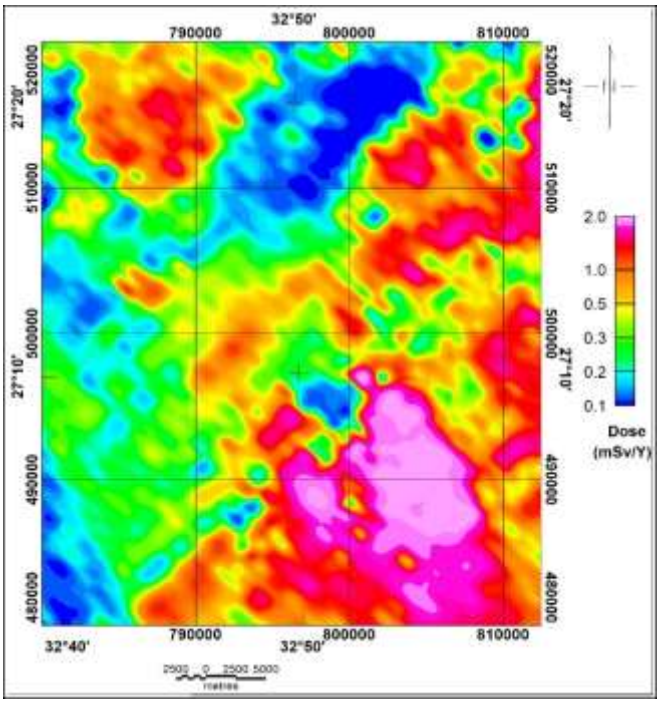

Fig.11: Dose rate filled colored contour map (in mS/Y), Wadi Hammad and vicinity area North Eastern Desert, Egypt.

d) Environmental Consequences of Gamma-Ray Spectrometric Data

In health physics, the radiation dose received by the tissue is of utmost importance. The energy that is delivered to the body is defined by the absorbed dose, which is expressed in units of Gray, rad, or Sievert. For a variety of reasons, it is very important to understand the nature and variability of environmental background levels of natural radiation. This information is crucial for the assessment of human exposure to such radiation and for the investigation of its pathological effects. Additionally, it offers fundamental details that can be used as a guide to spot and estimate the magnitude of any potential future changes in ambient radioactivity.

For the study area, the radiation dose rate map (Fig. 11) shows variable intensity values, ranging from 0.1 to 2 mSv/y, By comparison with the geologic map (Fig. 2), the lowest dose rate intensity levels were recorded over the Dokhan volcanic, Metavolcanics, Metasediments, Qusire Clastic member (Nubia Formation), and Tares sandstone member, while the intermediate level was recorded over the Metagabbro-Diorite complex, Hammamat sediments, and Dawi formation. The highest dose rate intensity levels, which are considered high levels of radiation, were recorded over the older granitoid younger granites, and post-granitic dykes.

According to the International Commission of Radiological Protection (ICRP) **[**20**]**, no person should absorb more than 50 milli-sieverts per year (50 mSv/y) from all natural and manmade radiation sources in their area. Currently, one mSv/y is the maximum recommended dose rate **[**21**]**. Regarding the study region, while the majority of the portions have dose rate intensity values greater than 1.0 mSv/y and may cause some harm to anyone located in these locations, other parts are still on the safe side and inside the maximum allowable safe radiation dose, posing no risk to the individual. The Metagabbro-Diorite complex, Hammamat sediments, Dawi formation, older granitoid, younger granites, and post-granitic dykes are primarily responsible for representing these locations.

4.2 Interpretation of the Airborne Magnetic Data

The airborne magnetic data of the study area has been subjected to classic and modern techniques of spectral and filtering analyses to describe the subsurface geological sources. The analyzed data was then used in a relatively precise interpretation to obtain the reconnaissance configuration of the subsurface geological layout of the investigated area. These techniques are the Reduce to the North Pole (RTP) and radially averaged power spectrum, to stand the average depths of shallow and deep sources and also to select the suitable cut-off frequency for carrying out both the high-pass (residual) and low-pass (regional) filtered maps; regional-residual separation through the application of high-pass and low-pass filters, to recognize the shallow and deep sources reasonable in the residual and

regional field; and upward continuation filter to complete the results of the previous filters and to enhance the deep features.

4.2.1 Qualitative Interpretation

a) Reduced to the Magnetic North Pole (RTP)

The magnetic values on the reduced-to-north magnetic pole (RTP) map (Fig. 12) typically range from -664 nT to 340 nT. It exhibits three magnetic anomaly zones (high, intermediate, and low). The research area's central, eastern, and north-eastern regions all have high magnetic anomalies. These anomalies are shaped linearly and lengthy. These high magnetic anomalies, which have directions of NW-SE, NNW-SSE, and E-W, are dispersed throughout the research area (Fig. 12).

Additionally, the northwestern and southwestern portions of high small scatter anomalies at various locations are circular or semicircular, linear, and elongated in shape (Fig. 12). The younger, older, granitoid granites and post-granitic dykes are associated with the high magnetic anomalies, either on the surface or below. The investigated area was covered in intermediate magnetic anomalies that ranged in color from yellow to green (Fig. 12). The surface geology indicates that these anomalies are connected to Wadi sediments, metavolcanic, and Dokhan volcanic metasediments. Low magnetic anomalies are shaped like ellipses and are both light and dark blue. These abnormalities occurred in the research area's southern, eastern central, and northernmost regions (Figure 12). They are a part of the Tares Sandstone Member, Qusire Clastic Formation, and Playa Deposits of the Wadi Formation in Nubia.

b) Power Spectrum Radially Averaged

On the RTP airborne magnetic map, where the regional and residual magnetic-component maps are acquired at 0.12 cycle/K-unit, a separation filter was implemented. Based on the power spectrum curve, the shallow and deep magnetic sources' estimated average depths are 800 m and 1800 m, respectively (Fig. 13).

c) Airborne Magnetic Maps, Residual and Regional

The residual magnetic anomalies can be defined as economically interesting anomalies because they indicate shallow anomalies and are characterized by weaker and more localized anomalies. The high-pass filtered (residual) magnetic map (Fig. 14) of the study area shows a successive system of magnetic dipoles all over the area with various amplitudes and frequencies. The local variation in frequency and amplitude of these anomalies may be due to differences in their composition and/or relative depth to their sources. These features have varying sizes, amplitudes, and frequencies.

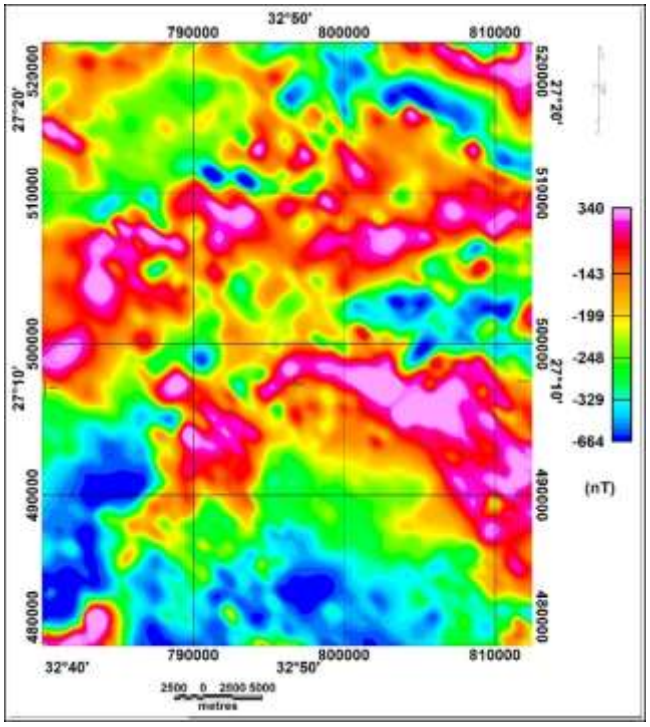

Fig. 12: RTP filled colored contour map (in nT), Wadi Hammad and vicinity area North Eastern Desert, Egypt.

Location of the 2D magnetic model.

Low pass filtered (regional) magnetic anomalies typically have high amplitudes and low frequencies and are strong, broad, stretch over large areas, and so on. These anomalies are of secondary interest in mineral exploration but of great significance in regional tectonic investigations of the basement complex. The research area's central, eastern, western, and southeastern regions all contain high

magnetic characteristics. Low magnetic characteristics are seen in the south and north, meanwhile. According to a good agreement between the high magnetic feature positions on the regional magnetic map and those on the residual and RTP maps, the causal magnetic bodies of these features have shallow depths and deep roots (Fig. 15).

d) Continued upward movement

The continuation process is the calculation of the potential field on a plane other than that at which it was observed. In principle, the field can be continued to different levels. The process by which magnetic field data are analytically projected from one data surface upward to level surfaces above the original data, i.e., mathematically transformed into what they would be if measured above the earth's surface, is known as upward continuation. It tends to accentuate anomalies caused by deep sources at the expense

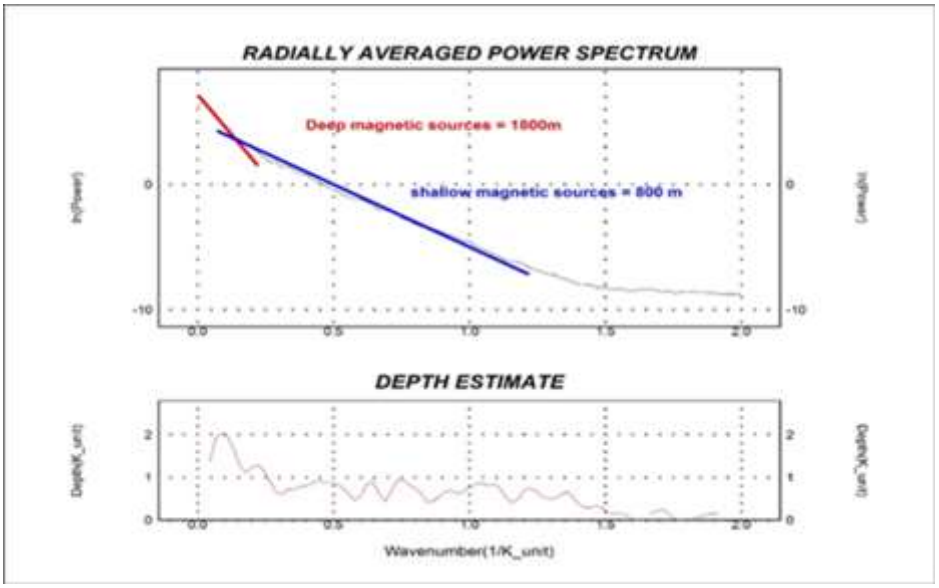

Fig. 13: power spectrum map, Wadi Hammad and vicinity area North Eastern Desert, Egypt.

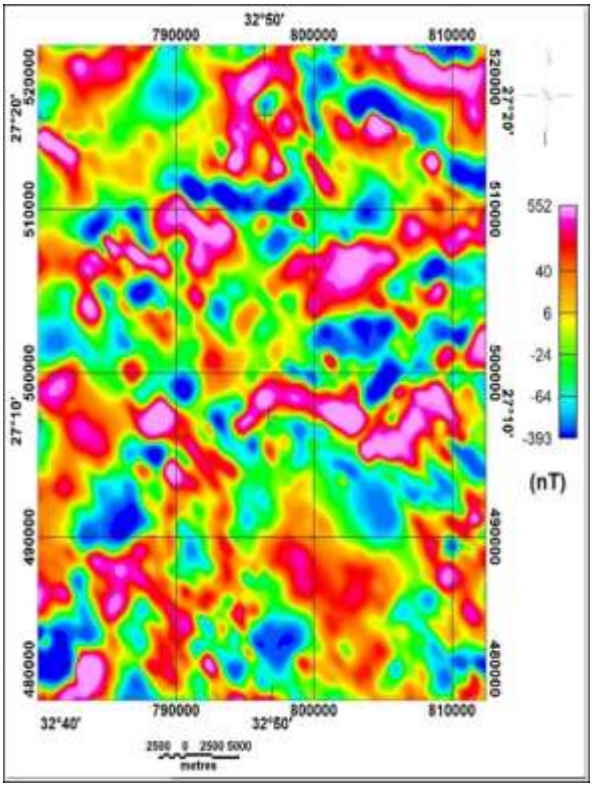

Fig. 14: Residual colored contour map (in nT), Wadi Hammad and vicinity area North Eastern Desert, Egypt.

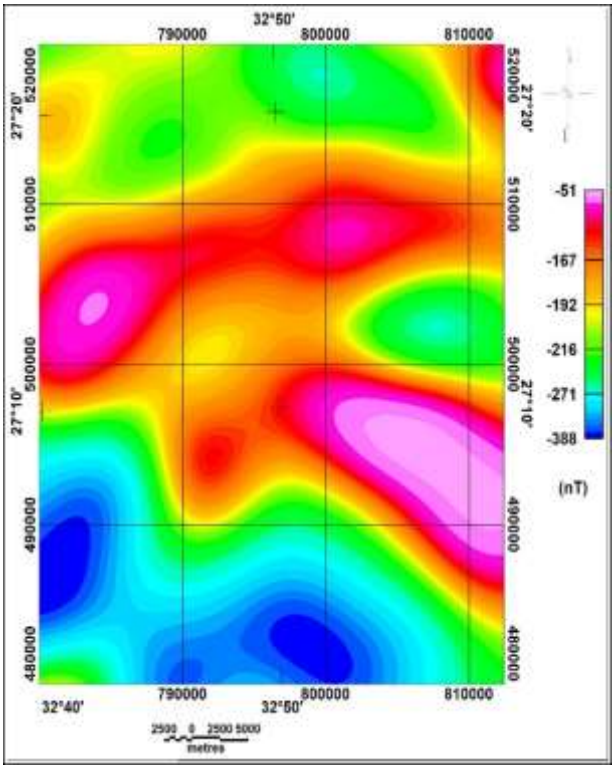

Fig.15: Regional colored contour map (in nT), Wadi Hammad and vicinity area North Eastern Desert, Egypt.

of those caused by shallow sources **[**22**]**. The result of upward continuation is the filtering of the magnetic effects of the deep-seated bodies from those of the near-surface ones. However, it may be desirable to remove or smooth out localized disturbances caused by features of the small lateral extent to bring out large-scale structures more clearly and give a clearer picture of the regional field **[**23**]**.

Investigation of the upward continued map at levels 100 Fig. (16), 400 Fig. (17), and 600 m Fig. (18) Show relatively the same character as the RTP map, while at level 1000 m, Fig. (19) reveals that most of the small-scale positive and negative anomalies that occurred on the RTP and high-pass (residual) maps have disappeared on this map. This observation would imply that the majority of the basement rocks, which are the source of magnetization in the area under study, are either exposed on the surface or are buried at a shallow depth close to it. Additionally, the upward-continued map at 1500 m altitude (Fig. 20). Several clusters of positive and negative magnetic anomalies with higher resolution than the RTP magnetic map are visible in Figure (20).

These anomalies are distinguished by their unusually high frequencies and short wavelengths, as well as their almost semicircular and elongated forms. At a level of 1500 meters, the ascending chart continued (Fig. 20) shows the existence of high and low magnetic anomalies, nearly at the same localities that have been observed on the upward continued map at level 600 m. Some of these magnetic anomalies are shown to be limited in extension, and other anomalies increase in extension at a depth of 1500 m. Moreover, some other anomalies are not obvious on the upward continued map at the fourth level (1500m), whereas they are still found on both the first, second, and third upward continued maps. According to this observation, these magnetic anomalies could have originated from depths of more than 1500 m to 1800 m (Fig. 21) and less than 2000 m Fig. (22), therefore, considered near-surface anomalies possessing shallow roots.

4.2.2. GM-SYS Magnetic Modelling

One profile was extracted from the RTP magnetic map perpendicular to the basin's major axes as shown in Fig. (12). The data was inverted using the GM-SYS software program and a 2D model was created. The maximum depth to the basement for this profile is 1500m, as deduced from the 2D model (Fig. 23) and the Werner deconvolution method (Fig. 24). Examination of the profile illustrates the following:

- The basement rocks in the studied area vary greatly in their composition, as reflected by the wide range of magnetic susceptibilities assigned to the different rocks.
- The modeling process indicates that the NE-SW basin is deeper towards the south.
- The southern portion of the basin is structurally more complex.
- Most of the high blocks along the profile are associated with high topography.
- Sub-topographic lows in the study area, along the modeled profile, are associated with subsided basement blocks with different throws. This result confirms well the interpreted troughs shown on the interpreted regional magnetic maps.

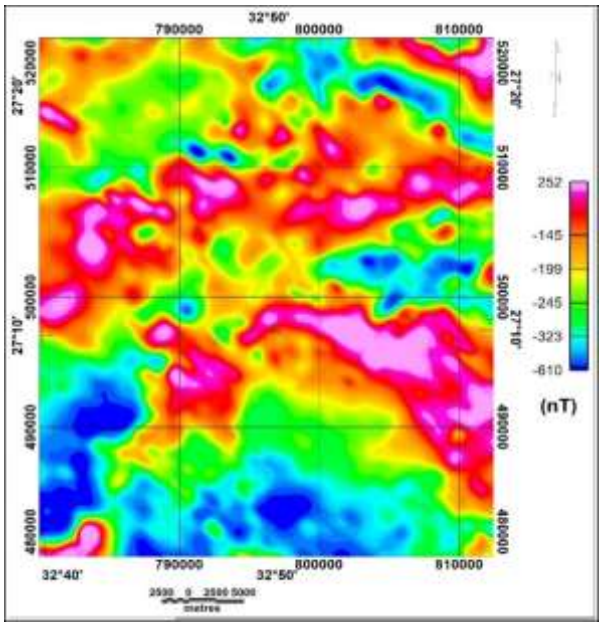

Fig. 16: Upward continuation colored contour map (100 m), Wadi Hammad and vicinity area North Eastern Desert, Egypt.

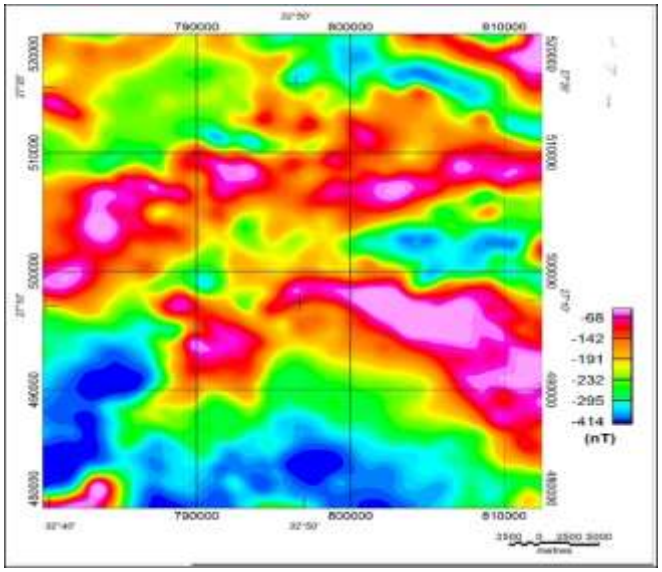

Fig. 17: Upward continuation colored contour map (400 m), Wadi Hammad and vicinity area North Eastern Desert, Egypt.

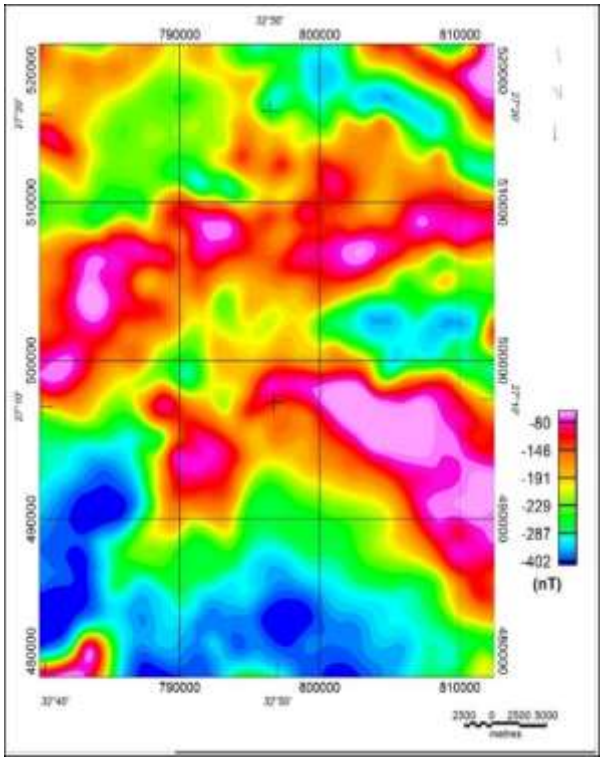

Fig. 18: Upward continuation colored contour map (600 m), Wadi Hammad and vicinity area North Eastern Desert, Egypt.

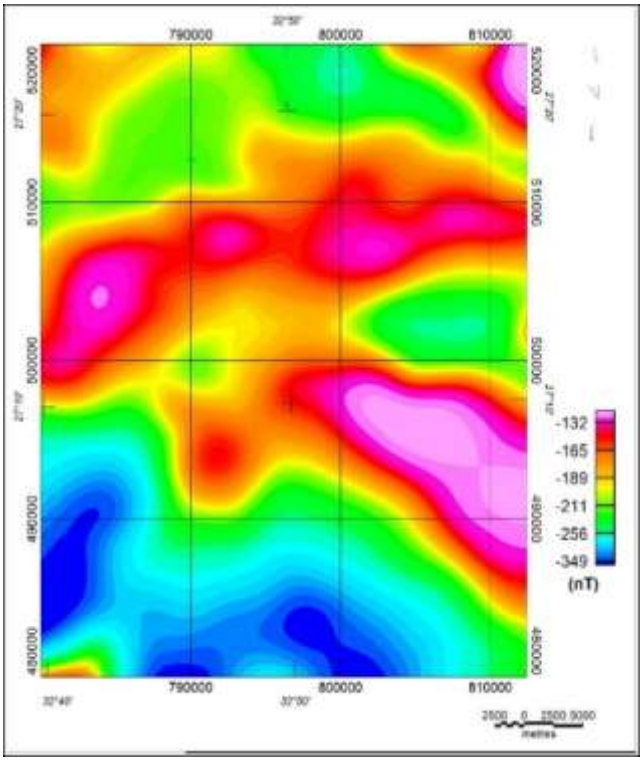

Fig. 20: Upward continuation colored contour map (1500 m), Wadi Hammad and vicinity area North Eastern Desert, Egypt.

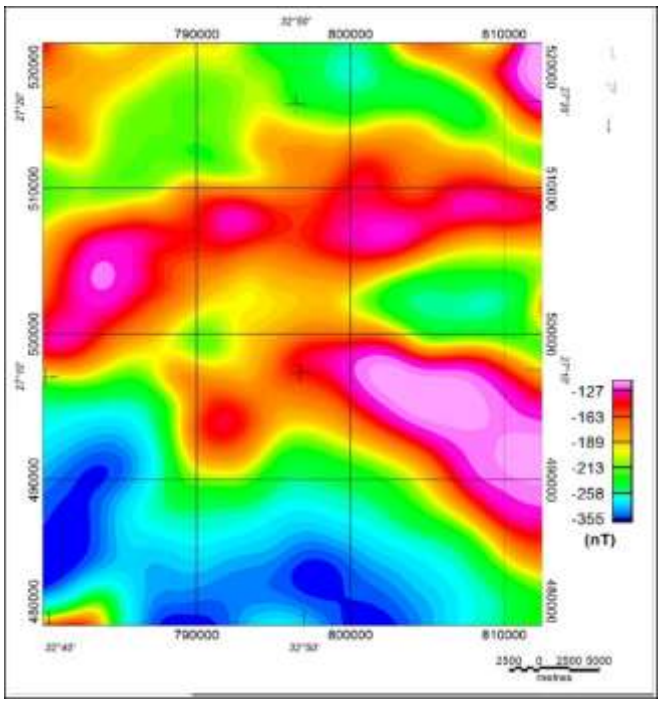

Fig. 19: Upward continuation colored contour map (1000 m), Wadi Hammad and vicinity area North Eastern Desert, Egypt.

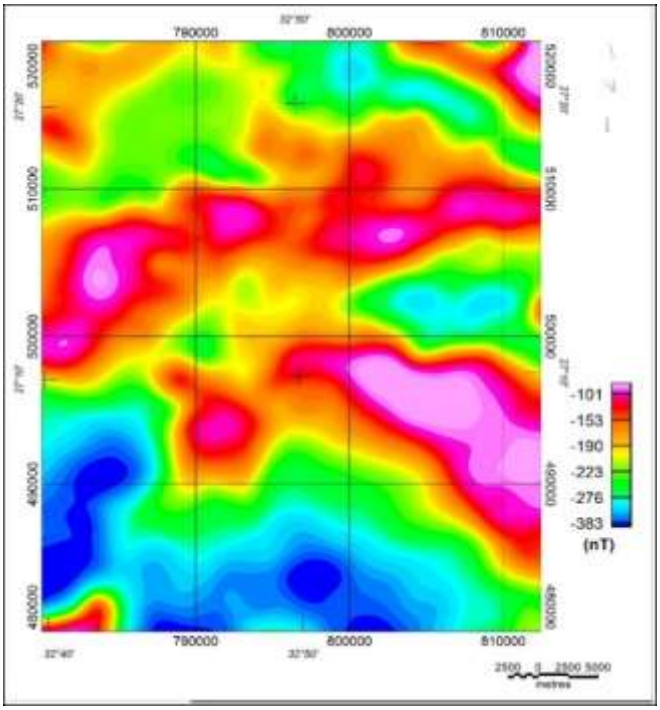

Fig. 21: Upward continuation colored contour map (1800 m), Wadi Hammad and vicinity area North Eastern Desert, Egypt.

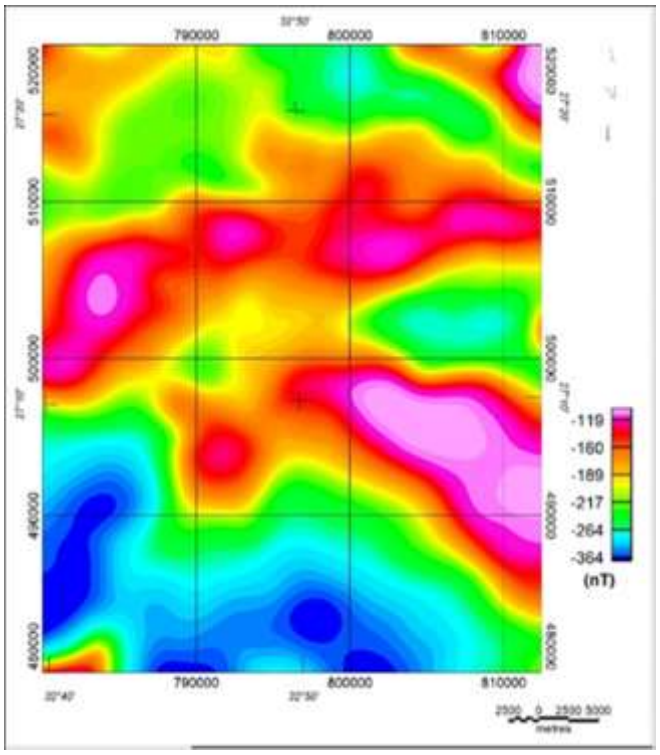

Fig. 22: Upward continuation colored contour map (2000 m), Wadi Hammad and vicinity area North Eastern Desert, Egypt.

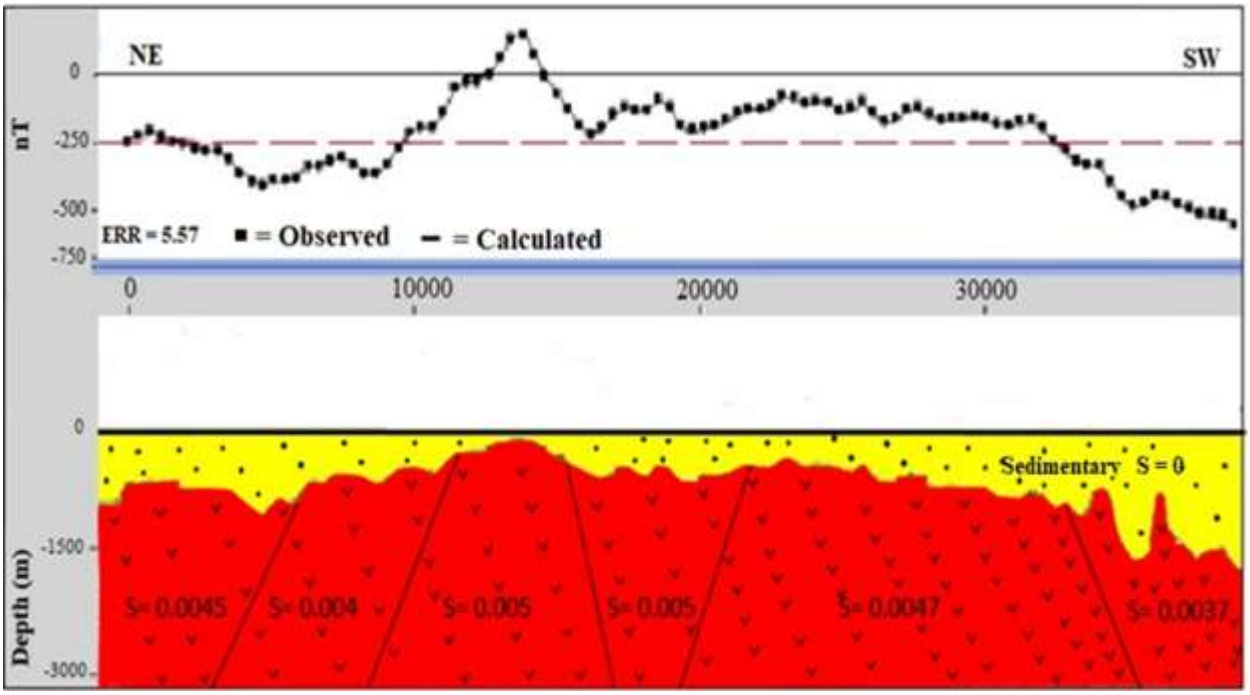

Fig. 23: The two-dimensional model of the magnetic profile, Wadi Hammad and vicinity area North Eastern Desert, Egypt.

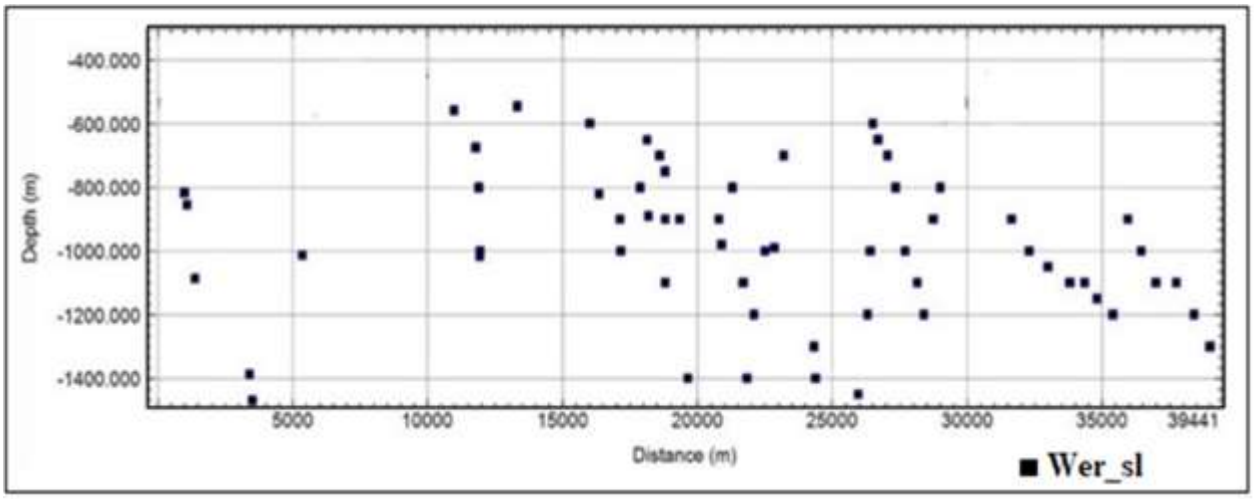

Fig. 24: Depths estimated by Werner deconvolution method, Wadi Hammad and vicinity area North Eastern Desert, Egypt.

4.3. Structural Lineament Analysis

In mineral exploration, where the majority of mineral resources are controlled by structures either directly or indirectly, structural lineament analysis is crucial. Surface, shallow, and deep lineament structures were derived from the RTP, residual, and regional maps to analyze the structural lineaments of the research area. As rose diagrams, these lineaments were displayed (Fig. 25).

Figures 25. a and 25. c, which shows rose diagrams of surface lineament structures, show that the typical tendencies are NW-SE, NE-SW, and E-W. These patterns might also be seen in the shallow and deep lineament structures' rose diagrams (Figures 25. c, e). This demonstrates that these tendencies persisted both above and below the surface. The rose diagram of the regional map (Figure 25. e) shows the N-S trend as the dominant structure, indicating that this trend is thought to be the deepest structure in the research area. The NE-SW and NW-SE trends are considered to be advantageous structures for mineral exploration, according to **[**24**]**.

The examination of RTP, residual, and regional structural maps (Fig. 25) reveals that the NNE-SSW, NE-SW, and NW-SE directions represent the primary structural trends in alteration zones. **[**25, 26**]** located seven spectrometric anomalies at El Gluf biotite granite in the southeastern part of the study area, and the distribution of these anomalies is related to faulting trends NS, NW, and NE.

The greatest influence on mineral exploration comes from structural lineaments because they serve as conduits for hydrothermal solutions that transport mineralization. Finally, when a suitable structural trap location is reached the solution deposit is loaded with mineralization, by this process the most important and famous vein-type uranium deposits are formed Salman et., al (1996). The primary goal of this investigation was to determine whether there was any correlation between structural lineaments and high radioactive zones. The results of this study demonstrate that there is an agreement between the structural lineaments and high radioactive zones, which is the main objective of this study **[**27-28**]**.

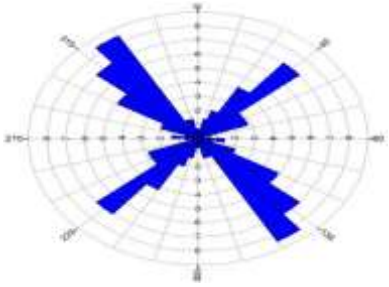

(a)Frequency

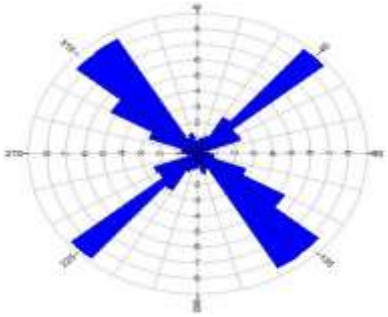

(b)Length

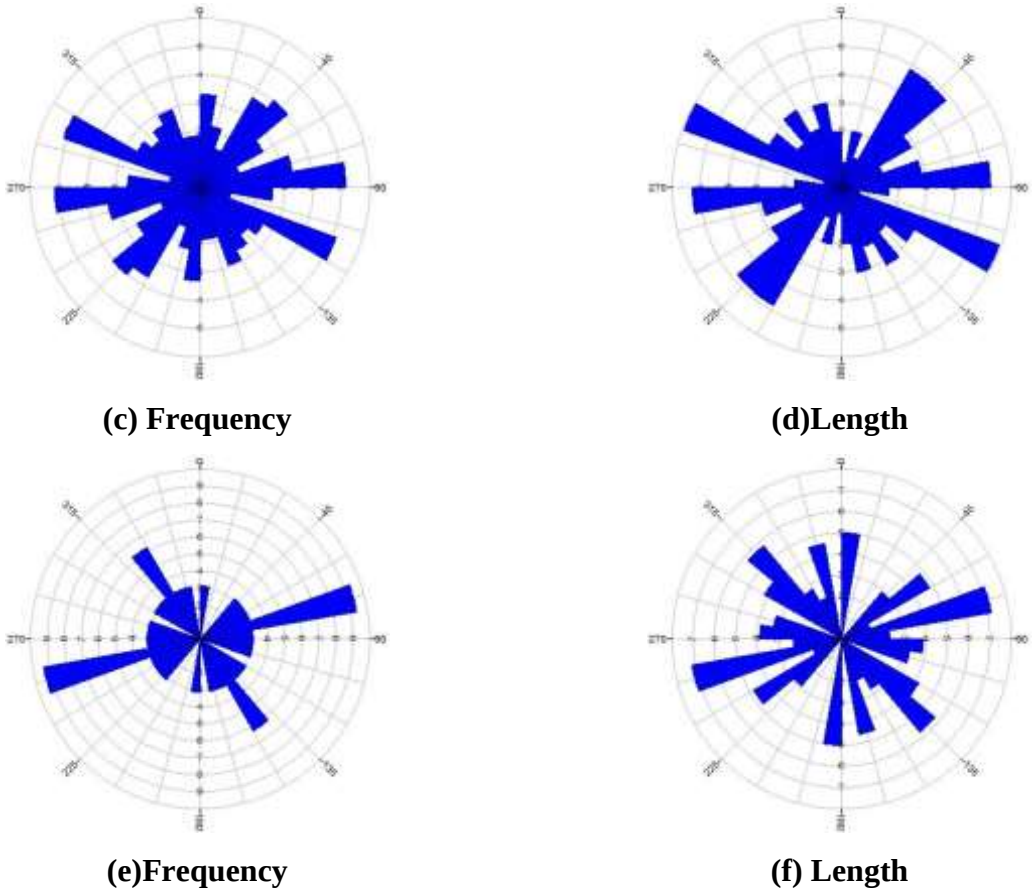

(c) Frequency **(d)Length**

(e)Frequency **(f) Length**

Fig.25: Rose diagrams of structural lineaments obtained from (a, b) RTP, (c, d) Residual, and (e, f) regional maps, Wadi Hammad and vicinity area North Eastern Desert, Egypt.

Acknowledgment: I would like to thank Prof. Salah Hanafi, Prof. Ahmed A. Nigm, and Prof. Ibrahim. M. Al Alfy and Dr. Hussein F. Abd-El Salam Nuclear Materials Authority, for kindly effort during this work.

Conclusions

For the research region, color image maps were used to illustrate the total count and concentration data for the three radioelements (K, eU, and eTh). These maps could provide a quick visual representation of the distribution of elevated radiation levels. The analysis of RTP, residual, and regional maps reveals the magnetic characteristics of rocks and the structural axes that may be connected to high radioactive zones. Additionally, the radially averaged power spectrum is used to estimate the depths of the shallow and deep magnetic anomalies. The following was discovered as a result of the use of several magnetic and spectrometric techniques:

The total count, eU, and eTh maps of the investigated area show a very broad range of radioactivity, with values ranging from around 2 to 20 Ur, 0.1 to 13 ppm, and 1 to 32, respectively. The highly white color seen in the radioelement composite image, which denotes an increase in the concentrations of the three radioelements in the area under investigation's northwestern, central, and eastern portions, is primarily associated with older granitoid younger granites and post-granitic dykes.

The examined areas had dose rate intensity values ranging from 0.1 to 2.0 mSv/y, which values more than 1.0 mSv/y may be harmful to anyone present there. The principal geologic features of these locations are the Hammamat-Diorite Complex, Hammamat Sediments, Dawi Formation, Older Granitoid, Younger Granites, and Post-Granite dykes.

According to the computed power spectrum of the RTP aerial magnetic data, the estimated average depths for shallow and deep magnetic causative bodies were 800 m and 1800 m, respectively.

An examination of the upward-continued maps reveals that the basement rocks, which are responsible for magnetization in the area under investigation, are either exposed or buried at a shallow depth close to the surface, and the magnetic anomalies may have their origins at depths of more than 1500 m to 1800 m and less than 2000 m.

Using a 2D model and the Werner deconvolution method, it was determined that the maximum depth to the basement for this profile is 1500m. The collected structural lineaments that impacted the research area were shown using rose diagrams. The radioactive mineralization process was significantly influenced by these structural lineaments.

The geology, RTP, residual, and regional maps for the research area were used to infer the structural lineaments, which were analyzed in the NNE-SSW, NW-SE, NE-SW, and N-S directions.

References

[1] Dobrin, M. B., and Savit, C. H., 1988. Introduction to geophysical prospecting. Mc Graw-Hill Book Company New York, 4th edition, 867p.

[2] Conoco, 1987.Geological map of Egypt, NF36 NW EI Sad Ali. Scale 1:500000. The Egyptian General Petroleum Corporation. Conoco Coral.

[3] Salman A.B., M.H.Shalaby and H.A.Khamis., 1996. Radiometric studies of Wadi Hammad area, North Eastern Desert, Egypt. Vol. of the 6th international conference nuclear science and applications 1996, Cairo, Egypt pp. 436-453.

[4] El-Sawy, E. K., Bekhiet, M. H., Abd El-Motaal, E., Orabi A. A. and Abd El Gany, M. K., 2011. Geo-environmental studies on Wadi Qena, Eastern Desert, Egypt: by using Remote Sensing data and GIS. Al-Azhar Bull. Sci. Vol. 22, No. 2 (Dec.): 33–60.

[5] Abdel Wahed, A.A., Ali, K.G., Khalil, M.M., Abdel Gawad, A.E., 2012. Dokhan Volcanics of Gabal Monqul area, Northeastern Desert, Egypt: geochemistry and petrogenesis. Arab J Geosciences 5:29–44. doi: 10.1007/s12517-010-0136-z

[6] Abdel Gawad, A.E.; Ali, K.G.; Wahed, A.A.A.; Alsafi, K.; Khafaji, M.; Albahiti, S.; Khalil, M.; Masoud, M.S.; Hanfi, M.Y., 2022. Excess Lifetime Cancer Risk Associated with Granite Bearing Radioactive Minerals and Valuable Metals, Monqul Area, North Eastern Desert, Egypt. Materials 2022, 15, 4307. https://doi.org/10.3390/ma15124307

[7] Fowler, A. and Osman, A. F., 2013. Sedimentation and inversion history of three molasse basins of the western central Eastern Desert of Egypt: Implications for the tectonic significance of Hammamat basins. Gondwana Research, 23, 1511-1534.doi:10.1016/j.gr.2012.08.022.

[8] Dessouky, O.K., Dardier, A.M., Abdel Ghani, I.M., 2018. Egyptian Hammamat molasse basins and their relations to arc collision stages: Implications for radioactive elements mineralization potential. Geological Journal, 54:1205–1222, DOI: 10.1002/gj.3220

[9] EI-Meliegy, M.A., El-Shayeb, H.M., Meleik, M.L. and Abdel-Raheim, R.M., 2000. Surface Delineation of Lithologies and Nomalies, Wadi Dib Area, Eastern Desert, Egypt, Using Aeroradiospectrometric Survey Data. Sci. J. Fac Sci. Minujiya Univ., VoL XIC: 179–231

[10] Ali, K.G., Eliwa, H.A., Masoud, S., Murata, M., Abdel Gawad, A.E., 2018. In: Structural Evolution of Wadi Road El-Sayalla Area, Eastern Desert, Egypt. News Ural State Min. https://doi.org/10.21440/2307-2091-2018-4-7-17. Univ. 7–17.

[11] Zaid, S.M., El-Badry, O.A. and Abdelaziz, Z.A., 2018. Diagenetic Aspects of the Nubian Sandstones, in the Central Eastern Desert, Egypt. World Applied Sciences Journal 36 (6): 789-798, DOI: 10.5829/idosi.wasj.2018.789.798.

[12] Moxham, R.M., Foot, R.S. and Bunker, C.M., 1965. Gamma-ray spectrometer studies of hydrothermally altered rock; Economic Geology.Vol.60, p.653-671.

[13] Charbonneau, B. W., Killeen, P.G., Carson, J.M. Cameron, G.W. and Richardson, K. A., 1976. Significance of radioelement concentration measurements made by airborne gamma-ray spectrometry over the Canadian Shield: IAEA Symposium on exploration for uranium ore deposits, Vienna, Austria, 1976, IAEA-SM 208/3, 35-53.

[14] Durrance, E.M., 1986. Radioactivity in geology. Principles and applications. Ellis Horwood Series in geology.xi+441 pp. Chichester: Ellis Horwood; distributed by John Wiley. ISBN 0 85312 761 1 (Ellis Horwood); 0 470 20389 7 (Halsted Press).

[15] Grasty, R.L., Mellander, Hand Parker, M., 1991. Airborne IAEA, 2000 gamma-ray spectrometer surveying. IAEA Technical Reports Series No.323.

[16] International Atomic Energy Agency (IAEA), 2003. Annual report covering the period from! st January to 31 December 2003, Vienna, Austria, 77p.

[17] Aero-Service, 1984. Final operational report of airborne magnetic/radiation survey in the Eastern Desert, Egypt for the Egyptian General Petroleum Corporation: Aeroservice, Houston, Texas, April 1984, 6.

[18] Neveen S Abed, Mohamed G El Feky, Atef El-Taher, Ehab El Sayed Massoud, Mahmoud R Khattab,

Mohammed S Alqahtani, El Sayed Yousef, Mohamed Y Hanfi 2022 Geochemical Conditions and Factors Controlling the Distribution of Major, Trace, and Rare Elements in Sul Hamed Granitic Rocks, Southeastern Desert, Egypt. Minerals 12 (10), 1245

[19] Awad, HAM., Zakaly, HMH., Nastavkin, AV., El-Taher, A., 2022 Radioactive content and radiological implication in granitic rocks by geochemical data and radiophysical factors, Central Eastern Desert, Egypt. International Journal of Environmental Analytical Chemistry, 102 (19), 7444-745.

[20 International Atomic Energy Agency (IAEA), 1979. "Gamma-ray surveys in uranium exploration". Technical reports series No. 186, IAEA, Vienna, Austria, 90p.

[21] International Atomic Energy Agency (IAEA), 2000. Annual report covering the period from! st January to 31 December 2000, Vienna, Austria, 187p.

[22] Blakely, R.J., 1995. Potential theory in gravity and magnetic applications. xix + 441 pp. Cambridge, New York, Port Chester, Melbourne, Sydney: Cambridge University Press. ISBN 052141508 X.

[23] Tasy, L. J., 1975.The use of the Fourier series method in upward continuation with new improvements. Geophysical Prosp., Vol. 23, pp. 28-41.

[24] Meshref, W. M., 1990. Tectonic framework of Egypt In Said, R. ed "The geology of Egypt" Balkema, Rollerdam, Printed in the Netherland., 734p.

[25] Ammar, A., A., El Kattan, E., M., and El-Sadek M. A. 1993. The distribution of radioelements in El Gluf biotite granite, North Eastern Desert, Egypt: a guide to the recognition anomalously radioactive zones. Journal of African Earth Science, Vol. 16, No, 4, pp. 473-488.

[26] El-Sadek, M. A. 1993. Geological interpretation of aerial spectrometric and magnetic survey data, Wadi-Hammad Qena area, Eastern Desert, Egypt. B. Sc., Ain Shams University, Cairo, Egypt, pp. 204.

[27] El-Taher, HA Madkour., 2014 Environmental and radio-ecological studies on shallow marine sediments from harbor areas along the Red Sea coast of Egypt to identify anthropogenic impacts. Isotopes in environmental and health studies. 2014, 50 (1), 120-

[28] Awad HA, Zakaly, HMH ., Nastavkin, AV., El Tohamy, AM., El-Taher, A., 2021 Radioactive mineralizations on granitic rocks and silica veins in the shear zone of El-Missikat area, Central Eastern Desert, Egypt. Applied Radiation and Isotopes. 2021, 168, 109493